An affordable pedagogical setup for wave-particule duality and applications to chaotic stadium cavity

Olivier Leblanc[1], Loïc Tadrist[2], Nicolas Moreau[1], Boris Brun-Barrière[1], Tristan Gilet[2], Benoît Hackens[1]
[1] NAPS/IMCN, UCLouvain, Louvain-la-Neuve, Belgium.
[2] Microfluidics Laboratory, GRASP, Department of Aerospace and Mechanics, University of Liege, B-4000 Liège, Belgium.

***Abstract*—Walking droplets represent an ideal playground to explore wave-particle duality at the macroscopic scale. Different experimental tools are required for a proper control and measurement of such a system which are often not easily affordable at undergraduate level. This paper proposes a complete low-cost and open-source experimental setup for walking droplets with a performance characterization. The setup is tested by examining droplets behaviour in the stadium billiard, a two-dimensional concave cavity that yields chaotic trajectories. Drastic differences between classical and quantum particles behaviour were observed in such geometry. It is observed that the walking droplet long-term evolution in a stadium billiard presents clear scarring patterns, informing on the existence of preferred "probable positions" within the billiard.**

***Index Terms*—Walking droplet, Stadium, Experimental setup, Low-cost**

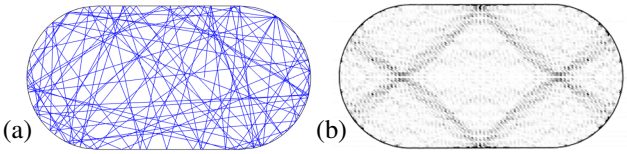

Fig. 1: (a) Simulated chaotic trajectory of a ball moving frictionlessly and bouncing elastically on the borders. (b) Scarred wavefunction : 2504th eigenmode for an electron confined in a stadium cavity with a size 18.14×9.07 [nm], obtained with the Pybinding tight-binding code in the "quantum_simulations" folder in [12].

I. Introduction

Wave-particle duality is probably one of the most peculiar aspects of quantum physics, which usually confounds students and newcomers in the discipline. It is intimately linked to the "measurement problem" which is at the heart of the Copenhagen interpretation of quantum mechanics [1]: according to this view, a measurement forces the wave function to collapse in only one of its possible values. The De Broglie theory, on the contrary of the Copenhagen interpretation, is a deterministic theory that associates a real pilot-wave that is created by the particle itself and guides its motion inside the space. It considers that the particle has, at any time, a definite and real position. This particle's position is practically unknown, but can be statistically predicted by the guiding equation [2]. In the De Broglie theory, the wave function obeying the Schrödinger equation is not real and is only representative of the averaged behaviour of the particle.

Human perception and apprehension of such complex topics is usually much easier when one can find analog macroscopic systems that can work as "toy models". Such analogs can help in the understanding and teaching of the different theories, but can also help test theories much more easily, if they can be implemented with simple experimental tools. In this context of wave-particle duality, a very interesting example of macroscopic analog was proposed by Y. Couder and coworkers in 2006 [3]. It consists in a silicone oil droplet bouncing on a bath vertically shaken with a sinusoidal vibration. With an appropriate set of forcing parameters (i.e. frequency and amplitude of the vertical shaking), this droplet can spontaneously start "walking" on the liquid surface (i.e. moving laterally) and in this case exhibits behaviours thought to be exclusive to the microscopic quantum realm such as self-organising lattice structures [4], single particle diffraction [3], quantized orbits [5,6], tunneling effects [7,8], and wave-like statistics in confined geometries [9–11] among others. A droplet spontaneously walking on the vibrated liquid surface is called *walking droplet*.

In this paper, we explore the behaviour of droplets walking inside a confined geometry: a stadium "billiard". The stadium billiard is a 2D geometry which consists in two semicircles separated along their axis of orthogonal symmetry, as shown in Fig. 1. This seemingly simple geometry was one of the first shown to be non-integrable (a.k.a. chaotic) despite the absence of concave borders by Bunimovich [13], and is thus also called Bunimovich stadium. The difference in behaviour between classical and quantum particles evolving in such cavities has raised scientific attention in recent decades. [14–17]. A classical particle moving in straight lines and bouncing elastically on the borders of the stadium generally[1] leads to unpredictable motion in practice despite the knowledge of the deterministic laws guiding its motion. The classical particle tends to visit the entire phase space [19] no matter its initial conditions. For a quantum particle (electron for instance) trapped in a stadium cavity, the stationary eigenmodes of the wavefunction $\Psi(\mathbf{r})$ give a non uniform probability of presence $|\Psi(\mathbf{r})|^2$ where $\mathbf{r}$ is the position inside the geometry. Furthermore, they concentrate in the vicinity of the unstable periodic orbits of the classical particle (one example is shown in Fig. 9(b)). These phenomena are known as *scars* and have been observed in various quantum systems [20–23].

In this context, given the contrasting behaviour between classical and quantum particles inside the stadium cavity, the central question of this paper is:

"How does a walking droplet behave inside a stadium cavity?".

Demonstrating that the walking droplet faithfully reproduces the electronic behaviour, for example, would provide an easy table-top solution for exploring complex physical problems related to electron dynamics, correlated electron behaviour, including many-body effects that are otherwise extremely difficult to reproduce through simulations.

The issue with performing accurate experimental observations with walking droplets is that it requires the implementation of several features such as the control of the vertical shaking, the imaging of both the horizontal and vertical droplet dynamics, and the droplet generation. Most research laboratories developed their

[1] Although there exists an infinite discrete set of unstable periodic orbits for the classical particle [18]

setup with costly equipment whose total cost reaches more than ten thousands euros. However, this cost is prohibitively high for a widespread use of such a setup, e.g. for teaching purposes.
In this paper, the creation of a complete low-cost ($<$ 200€) and open-source setup for observing walking droplets from scratch is discussed and compared with setups from research laboratories in Sec. II. All the data analysis routines and 3D conception drawings are available in [12].
The second part in Sec. III reports experimental observations of walking droplets inside stadium cavities of various sizes. In this framework, data from two different setups are compared : the low-cost setup mentioned above (*setup A*), and a "research setup" (*setup B*) at the University of Liège (ULiège, Belgium). It is observed that walking droplets generally converge towards surprisingly stable trajectories similar to some scarring patterns observed with quantum particles.

II. Low-cost Experimental setup

This section aims at describing the low-cost setup and justifying the choices made in its conception. The different software programs as well as 3D drawings made with *Solidworks* are available in open-source mode in [12]. The first citations of components in italic and cyan are clickable and linked to their datasheet. A schematic of the experimental setup is shown in Fig. 2(c). The different aspects are discussed in their dedicated sections below. A more detailed description can be found in [24].

A. Vertical shaking

A stadium-shaped bath made out of plexiglas has been fabricated and fixed on the membrane of a basic *loudspeaker*, playing the role of an electromagnetic shaker. The loudspeaker oscillates vertically with acceleration $\gamma(t) = \gamma_m \cos(\omega_0 t)$ where γ_m and $f_0 = \frac{\omega_0}{2\pi} = 80\text{Hz}$ are the prescribed maximum acceleration and frequency, respectively. The stadium width $W = 38\text{mm}$ and length $L = 2W = 76\text{mm}$ have been chosen such that $W \approx 8\lambda_F$, where λ_F is the Faraday wavelength, with the parameters in Table I. It is filled with silicone oil to a height $h_0 \in [6-11]\text{mm}$ (depending on the used stadium bath) such that a thin liquid film of depth $h_1 < 1.5\text{mm}$ overlays its border, serving as a wave damper. This choice instead of unsubmerged walls for delimiting the cavities allows to get rid of the additional waves that would have been generated by the meniscus at the walls [25]. The used silicone oil comes from *Sigma-Aldrich*, with its physical properties given in Table I. The viscosity $\nu = 20\text{cSt}$ at $T = 25°\text{C}$ has been shown to be ideal for observing walking droplets with a frequency of forcing $f_0 = 80\text{Hz}$ [26].
Following the dispersion relation of gravity-capillary waves [27], the liquid can be considered as having an infinite depth if the liquid height h_0 fulfils the condition :

$$\tanh(k_F h_0) \approx 1 \iff k_F h_0 > 4 \tag{1}$$

With the Faraday wavenumber $k_F = 2\pi/\lambda_F = 1330\text{rad/m}$, (1) yields the condition $h_0 > 3\text{mm}$ which will always be fulfilled inside the stadium in the following experiments.

The vertical forcing of the bath is ensured by a *NI Labview* program that communicates with a *NI myDAQ*. The electrical connections are shown in [24]. The *NI myDAQ* is able to actuate the loudspeaker through the use of a power amplifier, here a *Brüel Kjaer type 2706*. The loudspeaker has carefully been positioned horizontally. External vibrations are partly reduced using magnetic force and placing the bath on an anti-vibration foam. The acceleration measurement is performed using a 3-axis $\pm 16\text{g}$ *ADXL326 accelerometer*, which is supplied with 5V coming from a *Arduino Uno*. The accelerometer outputs a voltage in the range [0,3.3]V for each axis depending on the sensed acceleration in that direction. As there are only 2 analog inputs (AI) with the myDAQ, the X and Y accelerations are measured with the AI of the Arduino Uno. The measured sinusoidal forcing is shown in Fig. 3. Some harmonics can be observed in Fig. 3(b). The related total harmonic distortion (THD) is obtained as :

$$THD = \frac{\sqrt{\sum_{i=2}^{8} v_i^2}}{\sqrt{\sum_{i=1}^{8} v_i^2}} = 1.8\% \tag{2}$$

Where v_i is the amplitude of mode i in Fig. 3(b), $i = 1$ is the fundamental component at frequency $f = 80Hz$ and $i > 1$ are the harmonics, here considered up to $i = 8$. The transverse accelerations along X and Y axes are non-zero due to lack of stabilization of the cheap setup. They oscillate with the vertical forcing with an acceleration amplitude of $75 \cdot 10^{-3}\text{g}$ and $136 \cdot 10^{-3}\text{g}$, respectively.

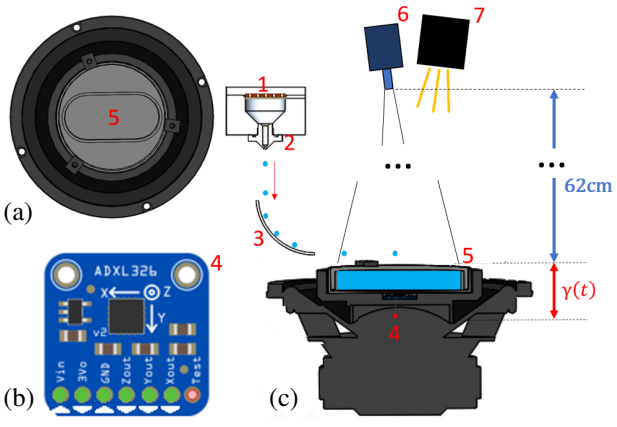

Fig. 2: *Setup A*. (a) Top view of the experiment as seen by the camera. (b) Accelerometer used for the acceleration measurement. (c) Schematic of the experimental *setup A*. 1 Piezoelectric- 2 Nozzle - 3 Launching pad - 4 Accelerometer - 5 Stadium - 6 Camera - 7 Lighting. The camera is placed at a height of 62cm.

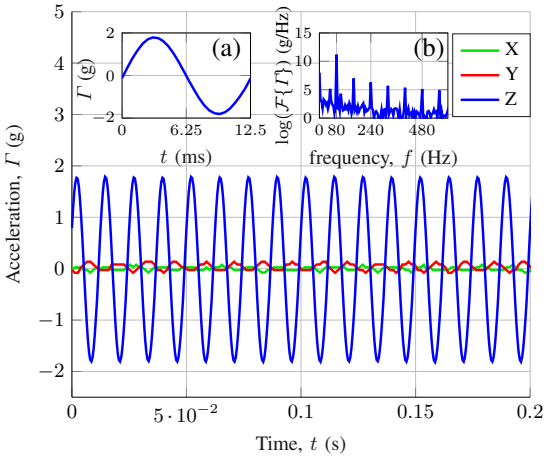

Fig. 3: Measured acceleration waveforms along X, Y and Z axes (green, red and blue curves, respectively). The resulting root mean squared error with respect to (wrt) a perfect sinusoid is $RMSE = 52.75 \cdot 10^{-3}\text{g}$. The inset (a) is a zoom on one period. The inset (b) shows the spectrum (i.e. Fourier transform $\mathcal{F}\{\Gamma\}$) of the acceleration in logarithmic scale.

TABLE I: **Properties and parameters.**

Name	Symbol	Value	Unit
SILICONE OIL			
Density	ρ	950	$\mathrm{kg/m^3}$
Kinematic viscosity	ν	20	$\mathrm{cSt{=}mm^2/s}$
Surface tension	σ	20.6	$\mathrm{mN/m}$
DROPLET			
Droplet diameter	D	$0.55-0.8$	mm
SHAKING FEATURES			
Frequency of forcing	f_0	80	Hz
Non-dimensional acceleration peak[a]	Γ	$3.8-4.5$	–
Faraday wavelength	λ_F	4.75	mm
Non-dimensional Faraday threshold[a]	Γ_F	$4.05-4.56$	–
Distance to Faraday threshold	$\mathcal{M}=\frac{\Gamma_F}{\Gamma_F-\Gamma}$	$8-500$	–
Memory [28]	$Me=0.765\mathcal{M}$	$6-380$	–

[a]Non dimensionalized by the acceleration constant $g=9.81\mathrm{m/s^2}$

B. Droplet generation

The droplet diameter is an important parameter which influences the walking droplet dynamics [29,30]. Inspired from [31], a piezoelectric *Droplet on-demand generator* (DOD), shown in Fig. 2, has been designed to produce droplets of repeatable diameter ranging from 0.5 to 1.4mm. By contrast with [31], no pump for regulating the pressure is used. The pressure equilibrium at the nozzle outlet is ensured by aligning it with the top of the fluid reservoir. The *piezoelectric buzzer* is activated with square voltage pulses generated by the switching of a bistable relay controlled by the Arduino Uno (see *Arduino_DOD_And_AccReading* in [12]). The voltage amplitude V_s and time width W_p are controlled by the Arduino Uno. The droplet diameter depends on V_s and W_p as well as on the nozzle outlet diameter n_D. The first two parameters are easily controlled with the computer. Models of nozzles to be 3D printed are proposed in [12] (Solidworks_Files/Louvain_la_Neuve folder). However, the DOD reservoir needs to be empty before the nozzle can be changed.

The droplet diameter measurements from top view images are shown in Fig. 4. From Fig. 4(a), it can be seen that averaging the diameter estimations over 10 selections or more leads to an error bar lying within the ± 0.02mm range. From Fig. 4(b), it can be seen that the variations of diameter between successive droplets generated with the DOD remain lower than 0.1mm.

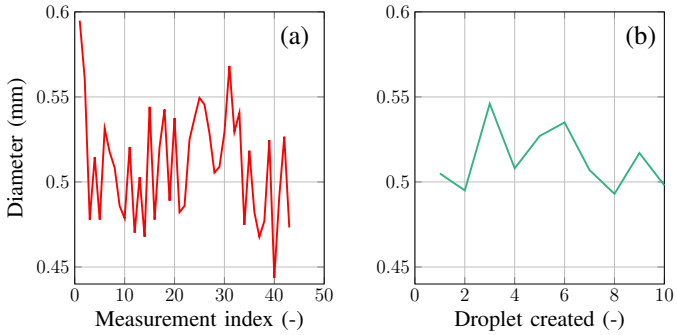

Fig. 4: (a) Estimations of the diameter of the same droplet on consecutive images. The measured mean and standard deviation over 43 measurements are $D_m=0.51$mm and $\sigma_D=0.032$mm, respectively. (b) Diameter of different droplets generated with the same parameters (nozzle of diameter $n_D=1$mm, voltage $V_s=50$V and pulse width Arduino command $W_p=4700\mu$s), each averaged over 20 different images.

C. Imaging the walking droplets

A proper imaging is essential for an accurate measurement of both droplet and wave dynamics. The imaging techniques implemented to measure the wave and droplet vertical dynamics are not covered as they are beyond the scope of this paper and matter less than the horizontal dynamics (i.e. in the stadium plane) for the question of this paper. The developed low-cost *setup A* has however been designed to handle such measurements, see discussion in [24]. From here, the analysis of droplet horizontal dynamics will be named *Droplet tracking* or *Droplet detection*.

Images of the pilot-wave system are recorded with a familial *Panasonic DMC-FZ45* camera, with a framerate of 25 FPS and a resolution of 1080x720 pixels. As shown in Fig. 2, it is placed above the bath at a height of 62cm. A desk lamp without occlusion is placed close to the camera and at the same height to avoid heating the liquid whose properties vary with temperature. The images are post-processed with *Matlab* routines available in [12] (*Visualization* folder). The criteria for an accurate droplet detection depend on the way the system is illuminated [24]. The configuration described here does not allow for a measurement of the wave dynamics but facilitates the tracking due to higher contrast between the walking droplet and the background. For consistency with the observations given in Sec. III, the droplet tracking results depicted in Fig. 5 come from *setup B* and have been obtained using Algorithm 1 in Appendix A. The tracking results obtained on *setup A* remain similar to the ones from Fig. 5 up to the camera resolution level.

The droplet detection in *setup B* simply consists in choosing the darkest pixel. By contrast, a more advanced detection criterium needs to be implemented in *setup A*. For each frame n, the droplet center $\mathbf{c}$ is chosen as the position maximizing $|g_n[x,y]|$ with :

$$g_n[x,y] = (\mathbf{I}_n|_{\mathcal{R}_n} - \mathbf{I}_{n-1}|_{\mathcal{R}_n})[x,y] \cdot \left(\{\mathbf{I}_{n-1}|_{\mathcal{C}_n}, \mathcal{R}_n\} \circledast \mathbf{I}_n|_{\mathcal{R}_n}\right)[x,y] \quad (3)$$

where $\mathbf{I}_n|_{\mathcal{R}}$ is the image at time frame n limited to the region of interest (ROI) $\mathcal{R}_n$, $\mathcal{C}_n$ denotes the correlation zone set of coordinates at time frame n. $\{\mathbf{I}_{n-1}|_{\mathcal{C}_n}, \mathcal{R}_n\}$ stands for the interpolation to the size of $\mathcal{R}_n$ using fast Fourier transform (FFT). The correlation operation $\circledast$ is computed via FFT for reducing the computational cost. In (3), the metric that is maximized is the combination (pointwise product) of an image difference (first line) and a correlation (second line).

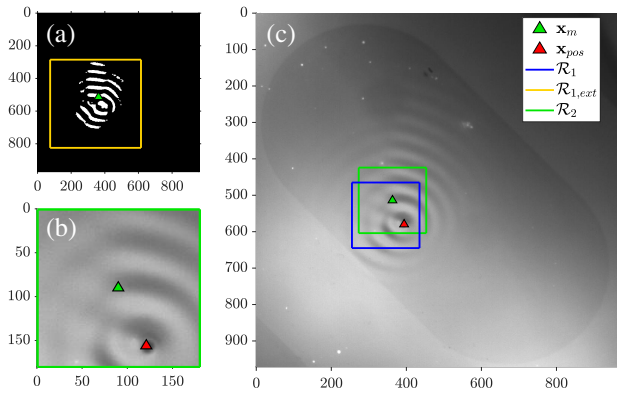

Fig. 5: Illustration of the droplet tracking using Algorithm 1 on *setup B*. (a) Binary mask $\mathcal{M}$ with it associated region of interest (ROI, orange frame) and center of mass (green triangle). (b) Zoom on $\mathcal{R}_2$. (c) Full processed image with the search ROIs.

D. Total cost

The desk lamp and the camera (a smartphone could be exploited) are likely already available for anyone thus no cost is associated. The cost contributions are depicted in Fig. 6. The *3D printing* part comprises the bath, reservoir and nozzles of the DOD. The silicone oil price does not correspond to the silicone oil from *Sigma-Aldrich* but cheaper versions on the market with less verification processes (e.g. on Amazon).

III. Walking droplet experiment

To illustrate the pedagogical power of the walking droplet experiment to teach wave-particle duality, experiments on walking droplet dynamics in stadium were conducted. Additionally, the validity of the low-cost *setup A* is checked through a comparison with results from *setup B*. An analysis of the stability of the attractor is finally given.

The experimental *setup B*, depicted in Fig. 7, comprises a circular shallow bath of diameter 24cm. Two baths stadium-shaped deep regions of various sizes (Fig. 7.(c-d)) have been used in the experiments. The experimental zones, i.e. the stadium cavities (in white) are filled with $h_0 \approx 4.2\text{mm}$ of silicone oil, also satisfying (1). The stadiums in Fig. 7.(d) have been placed far enough (min 22mm) to avoid any interaction [32]. The bath is placed on top of an electromagnetic shaker (V400LT, Data Physics). The shaker motion is accurately controlled via an accelerometer tightly fixed on the reservoir, a computer interface and a feedback loop, as detailed in [33]. The geometrical designs are available in [12] (*Solidworks_Files/Liege* folder).

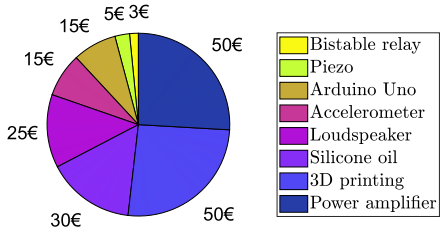

Fig. 6: Contributions to the total cost of 193€ for *setup A*.

TABLE II: Main differences between setups A and B.

	Setup A	**Setup B**
Bath size	10cm	24cm
Lighting	All from top desk lamp	Semi-refringent mirror high-power LEDs
Imaging - - **Resolution**	Basic camera non triggered / $\sim 60\mu\text{m/p}$	High-resolution camera triggered by $\gamma(t)$ Macro lens $\sim 120\mu\text{m/p}$
Shaking		PI controller
Anti-vibration	foam magnetic force	Springs included in the shaker
Insulation	/	Covering plate

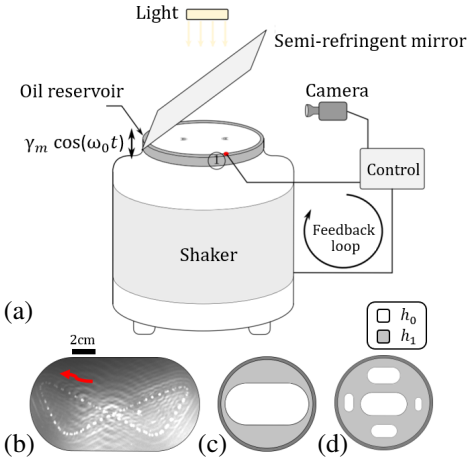

Fig. 7: (a) Experimental *setup B*. Schematic from [28]. (b) Top view of the deep experimental zone as seen by the camera. A superposition of multiple images is shown to highlight the droplet path. (c-d) Design of the stadiums mounted on the shaker.

The six different stadium zones will be written Ω_i with $i = 1, \ldots, 6$ ranging from largest to smallest. Their dimensions have been chosen wrt the Faraday wavelength $\lambda_F \approx 4.75\text{mm}$ and are shown in Table III. The only stadium from *setup A*, Ω_A, is also indicated.

The shaker is illuminated with 3 home-made high-power LEDs to obtain a uniform illumination of the bath. Thanks to a semi-refringent mirror placed at $45°$ above the shaker, optical paths of both illumination and recording are vertical near the bath surface. Thanks to a macro lens Zeiss Milvus 2/100M, the spatial resolution is brought down to $120\mu\text{m}$ by pixel for the less resolved images. The scene is imaged by a Basler acA2040 camera with 2040×2048 pixels resolution. The camera is triggered by a DACQ (National Instruments) and a Labview interface to capture one image every 500ms at the same phase wrt the droplet rebounds. The captured images are post-processed with Matlab to compute the droplet position following Algorithm 1 in Appendix A. For a fair comparison, the computed position coordinates are normalized in a reference stadium of dimensions 2×1 centered at the origin, as depicted in Fig. 8.

The following experimental results are accompanied by a triplet of parameter (Ω_i, D, Me) informing on the stadium used (see Table III), the droplet diameter (in mm) and the memory parameter (see Table I), respectively. The memory parameter [28] is defined as the

TABLE III: Stadium dimensions

Stadium	Ω_1	Ω_2	Ω_3	Ω_4	Ω_5	Ω_6	Ω_A
Radius $[\lambda_F]$	10	6	4	3	2	1.5	8

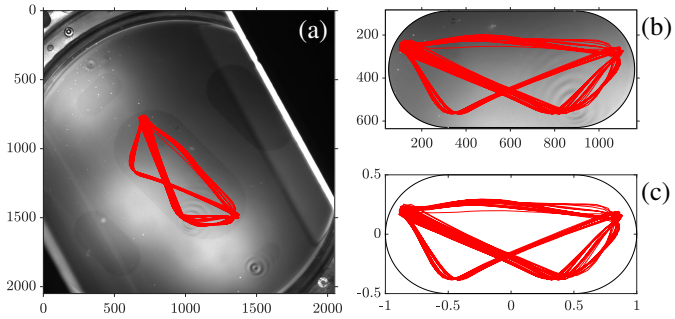

Fig. 8: (a) Trajectory in the original image. (b) Cutting out of the stadium and rotation up to horizontality. (c) Normalization of the trajectory.

ratio between the decay time constant τ and the Faraday period T_F :

$$Me = \frac{\tau}{T_F} = \frac{2\tau}{f_0} \tag{4}$$

It depends on the acceleration of the bath Γ induced by the vertical shaking as written in Table I. With the definition in (4), Me can be interpreted as the number of previous droplet bounces whose generated waves are still present on the liquid surface when the droplet bounces again.

The trajectories of walking droplets obtained with *setup A* and *setup B* are shown in Fig. 9(a) and Fig. 9(b), respectively. One observes similar trajectories for the two setups, showing the low-cost *setup A* described in Sec. II yields experimental results comparable to the more expensive *setup B*. Moreover, these trajectories respect the symmetries of the stadium geometry. Noteworthy, the trajectories remain stable through time, indicating they correspond to an equilibrium for wave-particle duality system, a.k.a. an *attractor*.

Fig. 10 compares the trajectories of a walking droplet with five different initial positions. For each of these experiments, the memory is gradually increased. The color gradient informs that the droplet starts walking from its initial position, with a gradual speed increase taking around 20s, as shown in Fig. 10(c). A periodic deceleration induced by the rebound of the walker on the stadium edges can also be seen in Fig. 10(c). It is observed that all the experiments converge towards the same trajectory of parallelogram-like shape after less than two interactions with the edges of the cavity. Only one loop inside the cavity is shown in Fig. 10(a) for the sake of clarity, but the stability of the attractor with time is highlighted in Fig. 10(b). The result shown seems to inform that the shape of the attractor is insensitive to the initial droplet position. Some observations not shown here also seem to indicate that the diameter D does not influence the shape neither.

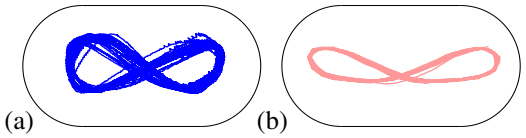

Fig. 9: (a) Trajectory obtained with *setup A*, 46 cycles overlap. $(\Omega_i, D, Me) = (\Omega_A, 0.8\text{mm}, 10)$ (b) Trajectory obtained with *setup B*, 19 cycles overlap. $(\Omega_i, D, Me) = (\Omega_3, 0.67\text{mm}, 165)$

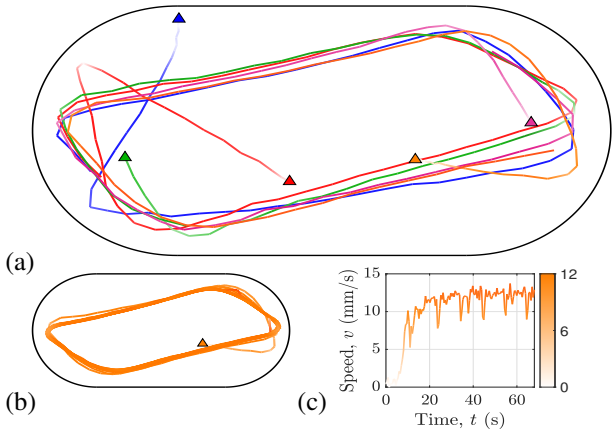

Fig. 10: $(\Omega_i, D, Me) = (\Omega_2, 0.77\text{mm}, 11.5)$ (a) Fast convergence of all initial conditions towards the same attractor. The triangles depict the initial position of the droplet. A color gradient whitens the line where the droplet speed is low. (b) One entire trajectory. 23 cycles overlap. (c) Droplet speed at early time.

IV. Conclusion and perspectives

A. Discussion on the results

A low-cost open-source experimental setup for observing walking droplets was presented, with satisfying performances and a reduction factor of the total cost around 50 with respect to conventional laboratory setups. The low-cost system may be improved by implementing a PI controller for the vertical shaking and adding a covering plate for insulation, i.e. protecting the system from parasitic air currents. The first observations of walking droplets inside stadium billiards were given. It was observed the wave-particle duality of walking droplets leads to stable trajectories similar to scarring patterns observed with electrons in the same geometry, and very different from the classical chaotic behaviour. The key parameters influencing this behaviour still need to be identified.

B. Perspectives for future research

This work opens many perspectives for further investigation in the comparison between the quantum world and the walking droplet pilot-wave system. First, the analysis could be deepened by comparing the 2D histogram of walking droplets inside the stadium cavities with the eigenmodes of the wavefunction $\Psi(\mathbf{r})$ inside a stadium billiard obtained by numerical simulations. Second, similar experiments could be performed in other chaotic geometries [13]. An analog to electron transport could also be studied by opening the stadium at one or multiple locations (*leads*), where the difference of potential between the leads would be translated in a difference of liquid depth, and an analog to conductance could be associated to the transmission probability between two different openings on the cavity's sides. This experiment would allow to look for a possible periodic dependence of the transmission on the difference of potential, analog to recurrence observed in electron transmission vs electron energy [20]. One could also imagine to add the analog of magnetic field by making the whole system turn around the vertical axis, and observe if the walking droplet trajectories become curved, until presenting a behaviour similar to the Quantum Hall Effect [34] where, in the quantum case, the particles tend to follow the borders of the billiard.

ACKNOWLEDGMENT

L. Tadrist (FNRS Grant No. CHAR. RECH.-1.B423.18 (Tadrist L.)), N. Moreau (FRIA fellowship), B. Barrière (research assistant) and B. Hackens (research associate) acknowledge financial support from F.R.S.-FNRS.

APPENDIX A
DROPLET TRACKING

The Algorithm 1 used for droplet position detection has been coded in *Matlab* and is available in [12].

Algorithm 1 Droplet tracking

Input: d
Output: $\mathbf{x}_{pos} \in \mathbb{R}^{N\times 2}$; ▷ Droplet positions
1: $\mathbf{I}_1 \leftarrow$ read() ; ▷ Initializations
2: $\mathbf{x}_{pos}(1,:) \leftarrow$ user_click()
3: $\mathcal{R}_1 \leftarrow \{\mathbf{x} = (x_1, x_2) : |x_i - \mathbf{x}_{pos}(1,i)| \leq d, i = 1,2\}$
4: **for** $n = 2$ **to** N **do**
5: $\mathbf{I}_n \leftarrow$ read()
6: $\mathbf{I}_{\text{diff},n} \leftarrow \mathbf{I}_{n-1} - \mathbf{I}_n$; ▷ Image difference
7: $\mathcal{M} \leftarrow \mathcal{H}(\mathbf{I}_{\text{diff},n}(\mathbf{x}))$, $\mathbf{x} \in \mathcal{R}_{1,\text{ext}}$; ▷ Hard thresholding
8: $\mathcal{M} \leftarrow RSPN(\mathcal{M})$; ▷ Denoising
9: $\mathbf{x_m} \leftarrow \mathrm{E}[\mathbf{x} \bullet \mathcal{M}]$, $\mathbf{x} \in \mathcal{R}_{1,\text{ext}}$; ▷ Center of mass
10: $\mathcal{R}_2 \leftarrow \{\mathbf{x} = (x_1, x_2) : |x_i - x_{m,i}| \leq d, i = 1,2\}$; ▷ ROI
11: $\mathbf{x_{pos}}(n,:) \leftarrow \arg\min_{\mathbf{x}\in\mathcal{R}_2} \mathbf{I}_n(\mathbf{x})$; ▷ Darkest pixel
12: $\mathcal{R}_1 \leftarrow \{\mathbf{x} = (x_1, x_2) : |x_i - \mathbf{x}_{pos}(n,i)| \leq d, i = 1,2\}$
13: **end for**
14: **return** $\mathbf{x}_{pos}$

Where d is half the size of the ROIs $\mathcal{R}_1$ and $\mathcal{R}_2$, $\mathcal{R}_{1,\text{ext}}$ is the extension of $\mathcal{R}_1$ to a half size of $2d$, $\mathcal{M}$ is a binary mask of the image dimensions, $RSPN$ stands for *Remove Salt And Paper Noise* using mathematical morphology tools [35], $E[\mathbf{x} \bullet \mathcal{M}]$ is the expectation operator applied on the masked positions and $\mathcal{R}_2$ is the ROI for the search of the minimum. The choice of the darkest pixel is motivated by the imaging technique described in Sec. III and shown in Fig. 5. Note only two consecutive images are stored in memory in each iteration unlike the implicit notations used in line 5 for the sake of clarity.

REFERENCES

[1] H. Pierce Stapp, "The copenhagen interpretation," *American Journal of Physics, vol. 40(8), pp. 51-80, (2009)*.
[2] Wikipedia contributors, "De broglie-bohm theory," https://en.wikipedia.org/wiki/De_Broglie-Bohm_theory, (2020), [Online; accessed 27-May-2020].
[3] E. Fort and Y. Couder, "*Single-Particle Diffraction and Interference at a Macroscopic Scale*," *Phys. Rev. Lett., vol. 97(15), pp. 154101, (2006)*.
[4] A. Eddi, A. Decelle, E. Fort, and Y. Couder, "*"Archimedean lattices in the bound states of wave interacting particles."*," *EPL (Europhysics Letters), vol. 87, 5, pp. 56002, (2009)*.
[5] A. U. Oza, M. Labousse, S. Perrard, and J. W. M. Bush, "*Pilot-wave dynamics in a harmonic potential: Quantization and stability of circular orbits*," *Phys. Rev. E., vol. 93, pp. 033122 (2016)*.
[6] E. Fort, A. Eddi, A. Boudaoud, J. Moukhtar, and Y. Couder, "*"Path-memory induced quantization of classical orbits."*," *Proceedings of the National Academy of Sciences, vol. 107, no. 41, pp. 17515–17520, (2010)*.
[7] L. Tadrist, T. Gilet, P. Schlagheck, and J. W. M. Bush, "*Predictability in a hydrodynamic pilot-wave system: Resolution of walker tunneling*," *Phys. Rev. E, vol. 102, pp. 013104, (2020)*.
[8] A. Eddi, E. Fort, F. Moisy, and Y. Couder, "*Unpredictable Tunneling of a Classical Wave-Particle Association*," *Phys. Rev. Lett., vol. 102(24), pp. 240401, (2009)*.
[9] T. Gilet, "*Quantumlike statistics of deterministic wave-particle interactions in a circular cavity*," *Phys. Rev. E, vol. 93, pp. 042202 (2016)*.
[10] D. M. Harris, J. Moukhtar, E. Fort, Y. Couder, and J. W. M. Bush, "*Wavelike statistics from pilot-wave dynamics in a circular corral*," *Phys. Rev. E, vol. 88, pp. 011001(R), (2013)*.
[11] T. Cristea-Platon, P. J. Saenz, and J. W. M. Bush, "*Walking droplets in a circular corral : Quantisation and chaos.*" *Chaos, vol. 28, pp. 096116, (2018)*.
[12] O. Leblanc. An affordable pedagogical setup for wave-particule duality and applications to chaotic stadium cavity. https://github.com/reivilo3/Walking-droplet-in-stadium-cavity.
[13] L. A. Bunimovich, "*On the Ergodic Properties of Nowhere Dispersing Billiards*," *Commun. math. Phys., vol. 65, pp. 295-312, (1979)* .
[14] E. J. Heller, "*Bound-State Eigenfunctions of Classically Chaotic Hamiltonian Systems: Scars of Periodic Orbits*," *Phys. Rev. Lett., vol. 53, pp. 1515, (1984)*.
[15] C. King, "*Exploring Quantum, Classical and Semiclassical Chaos in the Stadium Billiard*," *Quanta, vol. 3, pp. 16–31, (2014)*.
[16] R. Akis, D. K. Ferry, and J. P. Bird, "*Wave Function Scarring Effects in Open Stadium Shaped Quantum Dots*," *Phys. Rev. Lett., vol. 79, pp. 123, (1997)*.
[17] L. Huang, Y.-C. Lai, D. K. Ferry, S. M. Goodnick, and R. Akis, "*Relativistic Quantum Scars*," *Phys. Rev. Lett., vol. 103, pp. 054101, (2009)*.
[18] J. Lei and X. Li, "*Some dynamical properties of the stadium billiard*," *Physica D: Nonlinear Phenomena, vol. 189, Issues 1–2, 15, pp. 49-60, (2004)*.
[19] C. P. Dettmann, C. Orestis Georgiou P. Dettmann, and O. Georgiou, "*Transmission and reflection in the stadium billiard: Time-dependent asymmetric transport*," *Phys. Rev. Lett. E, vol. 83, pp. 036212, (2011)*.
[20] D. Cabosart, A. Felten, N. Reckinger, A. Iordanescu, S. Toussaint, S. Faniel, and B. Hackens, "Recurrent quantum scars in a mesoscopic graphene ring," *Nano Lett. 2017, vol. 17, 3, pp. 1344–1349, (2017)*.
[21] S. Sridhar, "*Experimental observation of scarred eigenfunctions of chaotic microwave cavities*," *Phys. Rev. Lett., vol. 67, no.1, pp. 785, (1991)*.
[22] T. Harayama, T. Fukushima, P. Davis, P. O. Vaccaro, T. Miyasaka, T. Nishimura, and T. Aida, "*Lasing on scar modes in fully chaotic microcavities*," *Phys. Rev. Lett. E, vol. 67, no.1, pp. 015-207, (2003)*.
[23] P. Wilkinson, T. Fromhold, L. Eaves, F. Sheard, N. Miura, and T. Takamasu, "*Observation of 'scarred' wavefunctions in a quantum well with chaotic electron dynamics*," *Nature, vol. 380, no. 6575, pp. 608–610, (1996)*.
[24] O. Leblanc, "Comparison between the walking droplet and the electron behaviour inside a chaotic stadium cavity," *Master thesis, UCLouvain, Belgium (2020)*.
[25] J. Bechhoefer, V. Ego, S. Manneville, and B. Johnson, "An experimental study of the onset of parametrically pumped surface waves in viscous fluids," *Fluid. Mech, vol. 288, pp. 325–350, (1995)*.
[26] S. Protiere, "*Gouttes rebondissantes : une association onde-particule à échelle macroscopique*," *phd thesis, Université Paris-Diderot - Paris VII, (2007)*.
[27] M. Phillips, "*The Dynamics of the Upper Ocean*."
[28] L. Tadrist, J.-B. Shim, T. Gilet, and P. Schlaghec, "*"Faraday instability and subthreshold Faraday waves: surface waves emitted by walkers."*," *J. Fluid Mech. (2018), vol. 848, pp. 906-945*.
[29] O. Wind-Willassen, J. Molacek, D. M. Harris, and J. W. M. Bush, "*"Exotic states of bouncing and walking droplets."*," *Physics of Fluids 25, 082002 (2013)*.
[30] J. Molacek and J. W. M. Bush, "*Drops walking on a vibrating bath : towards a hydrodynamic pilot-wave theory*," *J. Fluid. Mech., vol. 727, pp. 612-647, (2013)*.
[31] D. M Harris, T. Liu, and J. WM Bush, "*A low-cost, precise piezoelectric droplet-on-demand generator*," *Exp. Fluids, vol. 56(4), pp. 83, (2015)*.
[32] A. Eddi, E. Sultan, J. Moukhtar, E. Fort, M. Rossi, and Y. Couder, "*Information stored in Faraday waves: the origin of a path memory*," *J. Fluid Mech., vol. 674, pp. 433–463, (2011)*.
[33] N. Sampara and T. Gilet, "Two-frequency forcing of droplet rebounds on a liquid bath," *Phys. Rev. E, vol. 94, no. 5, pp. 53112–53120, (2016)*.
[34] Wikipedia contributors, "Quantum hall effect — Wikipedia, the free encyclopedia," https://en.wikipedia.org/wiki/Quantum_Hall_effect, (2020), [Online; accessed 11-June-2020].
[35] A. Ledda, "Mathematical morphology in image processing," *phd thesis, pp. 44, (2007)*.